Astronomy & Astrophysics manuscript no. 26993
October 22, 2015
©ESO 2015

arXiv:1510.06045v1 [astro-ph.SR] 20 Oct 2015

HE 0017+0055 : A probable pulsating CEMP-rs star and long-period binary ⋆

A. Jorissen[1], T. Hansen[2], S. Van Eck[1], J. Andersen[3,4], B. Nordström[3,4], L. Siess[1], G. Torres[5], T. Masseron[6], and H. Van Winckel[7]

[1] Institut d'Astronomie et d'Astrophysique, Université Libre de Bruxelles, CP 226, Boulevard du Triomphe, B-1050 Bruxelles, Belgium
e-mail: ajorisse@ulb.ac.be,svaneck@ulb.ac.be,lsiess@ulb.ac.be
[2] Landessternwarte, ZAH, Heidelberg University, Königstuhl 12, Heidelberg, D-69117, Germany
e-mail: thansen@lsw.uni-heidelberg.de
[3] Dark Cosmology Centre, The Niels Bohr Institute, University of Copenhagen, Juliane Maries Vej 30, DK-2100 Copenhagen, Denmark
e-mail: ja@astro.ku.dk, birgitta@astro.ku.dk
[4] Stellar Astrophysics Centre, Department of Physics and Astronomy, Aarhus University, DK-8000 Aarhus C, Denmark
[5] Harvard-Smithsonian Center for Astrophysics
60 Garden Street, Cambridge, MA 02138, USA
e-mail: gtorres@cfa.harvard.edu
[6] Institute of Astronomy, University of Cambridge, Madingley Road, Cambridge CB3 0HA, UK
e-mail: tpm40@ast.cam.ac.uk
[7] Instituut voor Sterrekunde, Katholieke Universiteit Leuven
Celestijnenlaan 200d - bus 2412, BE - 3001 Heverlee, Belgium
e-mail: Hans.VanWinckel@ster.kuleuven.be

Received / Accepted

ABSTRACT

Context. A large fraction of the carbon-enhanced extremely metal-poor halo giants ([Fe/H] < −2.5) are also strongly enriched in neutron-capture elements from the *s*-process (CEMP-s stars). The conventional explanation for the properties of these stars is mass transfer from a nearby binary companion on the Asymptotic Giant Branch (AGB). This scenario leads to a number of testable predictions in terms of the properties of the putative binary system and the resulting abundance pattern. Some among the CEMP stars further exhibit overabundances in r-process elements on top of the s-process enrichment, and are tagged CEMP-rs stars. Although the nucleosynthesis process responsible for such a mixed abundance pattern is still debated, these stars seem to belong to binary systems as do CEMP-s stars.

Aims. Our aim is to present and analyse in detail our comprehensive data set of systematic radial-velocity measurements and high-resolution spectroscopy of the CEMP star HE 0017+0055.

Methods. Our precise radial-velocity monitoring of HE 0017+0055 over 2940 days (8 yr) with the Nordic Optical Telescope and Mercator telescopes exhibits variability with a period of 384 d and amplitude of 540 ± 27 m s^{-1}, superimposed on a nearly linear long-term decline of ∼1 m s^{-1} day^{-1}. High-resolution HERMES/Mercator and Keck/HIRES spectra have been used to derive elemental abundances using 1-D LTE MARCS models. A metallicity of [Fe/H] ∼ −2.4 is found, along with s-process overabundances on the order of 2 dex (with the exception of [Y/Fe] ∼ +0.5), and most notably overabundances of r-process elements like Sm, Eu, Dy, and Er in the range 0.9 – 2.0 dex. With [Ba/Fe] > 1.9 dex and [Eu/Fe] = 2.3 dex, HE 0017+0055 is a CEMP-rs star. The derived atmospheric parameters and abundances are used to infer HE 0017+0055 evolutionary status from a comparison with evolutionary tracks.

Results. HE 0017+0055 appears to be a giant star below the tip of the red giant branch (RGB). The s-process pollution must therefore originate from mass transfer from a companion formerly on the AGB, now a carbon-oxygen white dwarf (WD). If the 384 d velocity variations are attributed to the WD companion, its orbit must be seen almost face-on, with $i \sim 2.3°$, because the mass function is very small: $f(M_1, M_2) = (6.1 \pm 1.1) \times 10^{-6}\ M_\odot$. Alternatively, the WD orbital motion could be responsible for the long-term velocity variations, with a period of several decades. The 384 d variations should then be attributed either to a low-mass inner companion (perhaps a brown dwarf, depending on the orbital inclination), or to stellar pulsations. The latter possibility is made likely by the fact that similar low-amplitude velocity variations, with periods close to 1 yr, have been reported for other CEMP stars in a companion paper (Jorissen et al., 2015). Moreover, Kiss & Bedding (2003) have shown that Wood's period-luminosity sequence D extends below the RGB tip, corresponding to periods of about 400 d, and is associated with velocity variations. A definite conclusion about the origin of the 384 d velocity variations should however await the detection of synchronous low-amplitude photometric variations.

Key words. Galaxy: halo – Stars: AGB and post-AGB – Stars: carbon – Stars: evolution – Stars: individual: HE 0017+0055

Send offprint requests to: A. Jorissen

⋆ Based on observations performed with the Mercator telescope and the Nordic Optical Telescope (NOT), operated by the Nordic Optical Telescope Scientific Association at the Roque de los Muchachos Observatory, La Palma, Spain, of the Instituto de Astrofïsica de Canarias.

1. Introduction

Over the past several years, evidence has been accumulating that as many as 20% of halo giants with [Fe/H] < -2.5 dex (a proportion rising to 80% at [Fe/H] ≤ -4.0 dex) exhibit overabundances of carbon by as much as 1−2 dex (the so-called *Carbon-Enhanced Metal-Poor* stars – CEMP stars; Beers & Christlieb 2005; Masseron et al. 2010; Placco et al. 2014). Moreover, stars with concomitant enhancement of *s*-process elements (CEMP-s stars) seem to preferentially inhabit the inner halo, while those without *s*-process enhancement (CEMP-no) stars seem to dominate the outer halo (Carollo et al. 2014). The conventional explanation for the origin of the CEMP-s stars is mass transfer from a nearby binary companion on the asymptotic giant branch (AGB) stage (which has since evolved into a white dwarf – WD), by Roche-lobe overflow or by a strong stellar wind, or possibly by a combination of both (Abate et al. 2013), in analogy with barium and CH stars (McClure & Woodsworth 1990). Indeed, preliminary radial-velocity data by Lucatello et al. (2005) suggested that most or all CEMP-s stars are long-period binaries, but the sample then available did not distinguish between CEMP-s and CEMP-no stars, and the results were not conclusive. We have therefore undertaken similar systematic studies to elucidate the origin of these stars in more detail. Simultaneously with the present study, Hansen et al. (2015b) addressed the same question, with the conclusion that 80% of CEMP-s stars are binaries, and CEMP-no stars are generally not. Besides CEMP-no and CEMP-s stars, there is another class of interest in the context of the present paper, namely the CEMP-rs stars. In addition to large overabundances of elements produced by the *s*-process, they also exhibit large overabundances of elements traditionally related to the *r*-process. The first such stars were discovered by Barbuy et al. (1997) and Hill et al. (2000). A number (if not all) of these stars exhibit radial-velocity variations (e.g., Sivarani et al. 2004; Barbuy et al. 2005; Hansen et al. 2015b). The nature of the companion star at the origin of the chemical enrichment of the CEMP star, probably through mass transfer, remains however debated (Masseron et al. 2010; Hansen et al. 2015b). An intermediate-mass AGB star where the ^{22}Ne(α,n)^{25}Mg neutron source operates is generlly invoked.

HE 0017+0055 was included in two independent radial-velocity monitoring programmes, one performed with the HERMES spectrograph attached to the 1.2-m Mercator telescope (Raskin et al. 2011) and addressing many different science cases (Van Winckel et al. 2010); the other with the fibre-fed, bench-mounted spectrograph FIES at the Nordic Optical Telescope (NOT); see Hansen et al. (2011). Given the unusual properties of HE 0017+0055, we decided to combine our data sets and discuss that star separately from the remainder of the samples (see Jorissen et al. 2015, for a discussion of the results of the HERMES monitoring of CEMP-s stars, and Hansen et al. 2015b, for a discussion of the NOT results).

HE 0017+0055 was discovered in a survey by Stephenson (1985) with a spectrum resembling type R, and received number 39 in the second edition of the *General catalog of Galactic carbon stars* (GCGCS; Stephenson 1989). It was later rediscovered in the framework of the Hamburg / ESO survey (Christlieb et al. 2001) as a high-latitude carbon star ($b = -61°$). Based on a fit of selected Ca and Fe lines (see Beers et al. 2007) with synthetic spectra, Kennedy et al. (2011) derived a metallicity of −2.7 for HE 0017+0055. Hence the star belongs to the family of CEMP stars.

The very low surface gravity ($\log g = 0.18$) adopted by Kennedy et al. (2011) for HE 0017+0055 would make it a very luminous CEMP star, a possible twin of CS 30322-023 (Masseron et al. 2006) and HD 112869 (Začs et al. 2015). Given the scarcity of such low-metallicity AGB stars, finding yet another example appears surprising and warrants the detailed study presented in this paper. In fact, based on the stellar parameters derived in Sects. 3 and 4, our study does *not* confirm, however, the AGB nature of HE 0017+0055, as we discuss in Sect. 5. But we start the paper by presenting the radial-velocity monitoring and the resulting orbital parameters (Sect. 2).

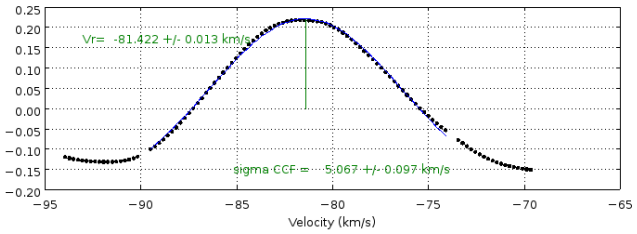

Fig. 1. A typical CCF for HE 0017+0055 from a spectrum taken with an exposure time of 900 sec. The vertical line shows the radial velocity of the star as derived from a Gaussian fit to the CCF core.

2. Radial-velocity monitoring and orbital solution

2.1. Radial-velocity monitoring with the HERMES spectrograph

The HERMES radial-velocity (RV) monitoring was performed with the fibre-fed HERMES spectrograph attached to the 1.2-m Mercator telescope of the Katholieke Universiteit Leuven, installed at the Roque de los Muchachos Observatory (La Palma, Spain) and fully described in Raskin et al. (2011). HERMES is designed to optimise both stability and efficiency and covers the whole wavelength range from 380 to 900 nm at a resolving power of ∼ 86 000. The high-resolution science fibre has a 2.5 arcsec aperture on the sky, using a two-slice image slicer.

A Python-based pipeline extracts a wavelength-calibrated and a cosmic-ray cleaned spectrum. A separate routine is used for measuring RVs, by means of a cross-correlation with a spectral mask constructed from a carbon-star spectrum. A restricted region, covering the range 478.11 – 653.56 nm (orders 55 – 74) and containing 2103 useful spectral lines, was used to derive the RV, in order to avoid telluric lines on the red end and crowded and poorly-exposed spectra on the blue end. A spectrum with a signal-to-noise ratio of 15 is usually sufficient to obtain a cross-correlation function (CCF) with a well-pronounced maximum. A typical CCF is shown in Fig. 1 for a spectrum with a SNR of 15 in the selected spectral region.

Radial velocities are determined from a Gaussian fit to the core of the CCF with an internal precision of a few m/s. The most important external source of error is the varying atmospheric pressure in the spectrograph room (see Fig. 9 of Raskin et al. 2011), which is largely eliminated by the arc spectra taken for wavelength calibration. The long-term stability (years) of the resulting radial velocities is checked with RV standard stars from Udry et al. (1999). Their standard-deviation distribution peaks at $\sigma(Vr) = 55$ m/s (see also Fig. 2 of Jorissen et al. 2015), which we adopt as the typical radial-velocity uncertainty for such relatively bright stars. The RV standard stars have also been used to tie the HERMES RVs to the IAU standard system.

The list of HERMES velocities is given in Table 1.

Table 1. HERMES/Mercator and FIES/NOT radial velocities of HE 0017+0055 (without any zero-point correction). The uncertainty quoted on the FIES RVs corresponds to the standard deviation of the correlation results from all spectral orders. For the HERMES data, the uncertainty is instead the formal error on the CCF Gaussian fit on 20 orders. A more realistic uncertainty is the long-term error describing the long-term stability of the spectrographs (see text).

JD (-2 400 000)	$Vr \pm \epsilon$ (km s^{-1})		JD (-2 400 000)	$Vr \pm \epsilon$ (km s^{-1})	
HERMES			NOT		
55053.5756	-79.423	0.008	54314.6702	-78.622	0.007
55053.5890	-79.431	0.005	54338.6419	-78.944	0.007
55053.6025	-79.382	0.009	54373.6224	-78.691	0.009
55087.5807	-79.899	0.011	54396.5371	-78.583	0.007
55087.5939	-79.823	0.006	54406.5966	-78.505	0.012
55087.6072	-79.851	0.006	54480.3868	-78.183	0.012
55098.6838	-79.597	0.008	54793.4846	-79.098	0.018
55098.6976	-79.590	0.006	54820.3386	-78.830	0.017
55098.7124	-79.738	0.007	55059.7365	-79.922	0.008
55159.5055	-79.417	0.006	55149.4730	-79.647	0.010
55159.5201	-79.429	0.006	55207.3499	-79.391	0.015
55159.5343	-79.463	0.014	55415.6081	-80.439	0.009
55418.6223	-80.099	0.008	55439.5914	-80.778	0.010
55423.7016	-80.118	0.003	55503.4086	-80.330	0.023
55497.4806	-79.992	0.007	55738.7344	-80.148	0.008
55938.3316	-79.977	0.008	55776.6821	-80.675	0.008
55956.3373	-79.944	0.003	55821.5766	-80.870	0.009
56109.7113	-80.056	0.005	55944.3253	-80.429	0.011
56140.7386	-80.201	0.006	56139.7129	-80.857	0.010
56311.3363	-80.588	0.007	56241.3910	-81.420	0.018
56481.7027	-80.278	0.007	56545.6267	-81.474	0.011
56511.7176	-80.560	0.007	56652.4180	-81.951	0.015
56557.6467	-80.868	0.006	56686.3209	-81.538	0.015
56634.3763	-81.416	0.007	56840.7182	-80.866	0.028
56849.6608	-80.395	0.017	56888.5421	-81.261	0.013
56904.6038	-80.550	0.016	56917.5981	-81.398	0.014
56947.5245	-80.919	0.014	56987.3813	-81.885	0.009
56994.3660	-81.219	0.013	57257.5774	-81.396	0.010
56996.3424	-81.103	0.012			
57052.3396	-81.528	0.005			
57052.3506	-81.422	0.013			
57056.3370	-81.287	0.018			
57056.3498	-81.274	0.017			

2.2. Radial-velocity monitoring at the NOT

The NOT spectra were obtained in service mode at roughly monthly intervals with the FIES spectrograph[1], which covers the fixed wavelength range 364 nm − 736 nm in 78 orders at a resolving power of $R \sim 46\,000$. The average SNR of the spectra is ∼10, ranging from ∼2 to ∼20, and is obtained in ∼20 min on a star of $V = 14.5$. Integrations of 15 min or longer are split into three in order to enable effective cosmic-ray rejection, and a Th-Ar reference spectrum is observed immediately before every stellar spectrum. 2 − 3 RV standard stars from a fixed set of seven, also selected from Udry et al. (1999), were observed on every observing night in order to monitor any zero-point variations in the derived velocities.

[1] http://www.not.iac.es/instruments/fies/

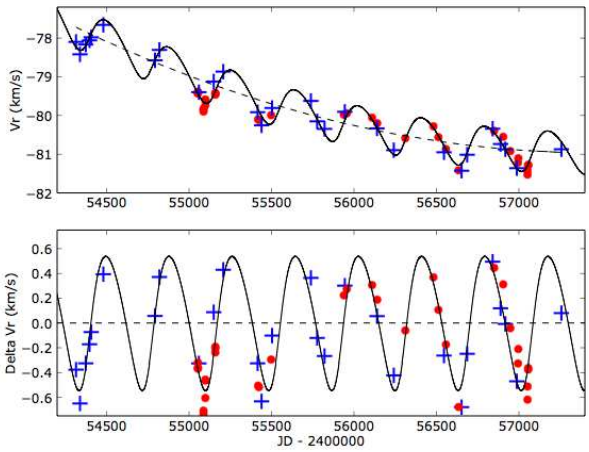

Fig. 2. The radial-velocity curve of HE 0017+0055 showing the short- and long-term orbital fits combined (top) as well as the short-term orbit alone (red dots: HERMES velocities; blue plusses: NOT velocities).

The observations were reduced and correlated with software developed by Lars Buchhave, originally to deliver high-precision radial velocities of exo-planet host stars from echelle spectrographs, especially from FIES (Buchhave et al. 2010). Using the highest-signal spectrum of HE 0017+0055 itself as the template spectrum, multi-order cross-correlation and optimised filtering is performed, and the final radial velocity, given in Table 1, is determined by a Gaussian fit to the peak of the CCF. The internal error of each velocity, also listed, is the standard deviation of the results from all spectral orders. Correlation with a "Delta" template, a synthetic spectrum consisting of δ functions at the (solar) wavelengths of selected lines, is used to determine the radial velocity of the HE 0017+0055 template and thus that of the whole data set. More details are given in Hansen et al. (2015b), from where the NOT data in Table 1 are taken.

The observations of the (much brighter) RV standard stars were reduced exactly as for all science targets. The typical standard deviation is 38 m s^{-1} for a star with ∼41 observations over ∼2700 days, or 7.5 years, and the mean differences between the NOT and Udry et al. (1999) radial velocities is -13 ± 38 m s^{-1}.

The velocity curve from the combined HERMES+NOT data set covers 2943 days or 8 years with a mean radial velocity of ~ -80 km s^{-1}. It is presented in Fig. 2, which clearly shows 8 cycles of a short-term periodic velocity oscillation, superimposed on a long-term trend. We have found that the latter is best modelled by a quadratic polynomial of the form $Vr = 3.252 \times 10^{-7} x^2 - 0.0374x + 993.215$, where $x = JD - 2400000$, while the short-term oscillation is adequately represented by a Keplerian orbit.

2.3. Orbital solution

From trial orbital solutions of the separate HERMES and NOT, we found that adding a small zero-point correction of 0.52 km s^{-1} to the NOT velocities would minimise the standard deviation of the merged data set in the combined orbital solution, the elements of which are given in Table 2. Fig. 2 shows the velocity curve from the complete HERMES+NOT data set as well as the short-term orbit alone.

Table 2. Orbital elements of the presumed short-period pair.

P (d)	384.6 ± 0.9
e	0.15 ± 0.04
ω (°)	234 ± 16
T_0	2455908.0 ± 15.7
V_0 (km s^{-1})	0.04 ± 0.02
K (km s^{-1})	0.54 ± 0.03
$f(M_1, M_2)$ ($M_\odot$)	$(6.1 \pm 1.1) \times 10^{-6}$
$a_1 \sin i$ (Gm)	2.8 ± 0.2
σ (km s^{-1})	0.14
N	61

Note. The table lists the orbital parameters, as follows: P is the orbital period; e is the orbital eccentricity; ω is the argument of periastron; T_0 is the time of passage at periastron; V_0 is the velocity of the barycentre; K is the semi-amplitude of the orbit: $f(M_1, M_2)$ is the mass function; a_1 is the semi-major axis of the orbit of the visible component around the centre of mass of the system; i is the inclination of the orbital plane with respect to the plane of the sky; σ is the rms of the $O - C$ residuals; N is the number of data points.

With the highly significant radial-velocity amplitude and stable period over eight orbital cycles, and in absence of any photometric evidence for stable pulsations (this aspect will be further discussed in Sect. 2.4.3 in relation with Fig. 3), it seems natural to interpret our velocity data as implying that HE 0017+0055 is a triple star system with an inner orbit of low eccentricity (which is either seen nearly face-on, or with a low-mass companion) and a more distant companion. These alternatives will be discussed in the next section (Sect. 2.4). Note that the shorter period is sufficiently different from 365 d that phases have shifted by about half a cycle over the 8-year span of our monitoring, relative to any residual seasonal effects, and we have documented elsewhere (Hansen et al. 2011) that we can reliably measure binary motions of similar period and even lower amplitude. The outer orbit must have a period of several decades, since we only see marginal evidence of a gradual acceleration over $\sim$ 3000 d.

Considering the fact that HE 0017+0055 is a CEMP-rs star (as we will show in Sect. 4), not residing on the AGB (see Sect. 5 and Fig. 8), it must owe its peculiar abundances to mass transfer in a binary system, like barium and CH stars (McClure & Woodsworth 1990; Gorlova et al. 2013; Jorissen et al. 2015). The most recent collection of orbital elements for these families, presented in the two recent references above, indicates that their orbital periods range between 80 d and up to 50 yr or more. Both the inner and outer companions of HE 0017+0055 have periods in this range, consistent with that of barium and CH systems. This argument based on orbital periods cannot be used thus to tag which, among the inner or outer companion, is the WD responsible for the chemical pollution. In case the short-period variations turn out not to be of Keplerian origin (as we will argue in Sect. 2.4.3), the long-term velocity variations must then be attributed to the WD companion. As discussed above, this poses no problem in terms of accretion efficiency, since orbital periods of several decades are known among CH and barium stars.

2.4. Origin of the short-term velocity variations

The remarkable feature of the short-term orbit presented in Table 2 is the very small value of its mass function [$(6.1 \pm 1.1) \times 10^{-6}$ $M_\odot$]. In this section, we discuss three possible interpretations of this fact: (i) an orbit with a very low inclination; (ii) a companion of very low mass; (iii) a spurious Keplerian solution, the velocity variations being caused by envelope pulsations.

2.4.1. An orbit with a very low inclination?

The small mass function derived from the orbital fit could imply a very low orbital inclination. Assuming $M_1 = 0.9$ $M_\odot$ for the primary component of HE 0017+0055, $i \sim 2.3°$ is required to yield a secondary mass of $M_2 = 0.6$ $M_\odot$, typical for a CO WD. In this situation, it is thus the inner companion which is responsible for the chemical pollution, whereas the outer companion is an innocent bystander. This situation immediately implies that the two orbits cannot be co-planar. If they were so, the semi-amplitude of the outer orbit (assumed to be 3 km s^{-1}; Fig. 2), the inferred inclination (2.3°) and period ($\sim 4 \times 8 = 32$ yr) would imply a mass of several 10^3 $M_\odot$ for the outer companion, which is of course impossible. Indeed, many non-coplanar triple systems are known (Hummel et al. 2003; Muterspaugh et al. 2008; O'Brien et al. 2011), and modern theories of stellar formation (Sterzik & Tokovinin 2002; Fabrycky & Tremaine 2007) predict that triple systems will form non-coplanarily.

2.4.2. An orbit with a very low-mass companion?

An alternative solution is that of a very low-mass companion. If $M_1 = 0.9$ $M_\odot$ as assumed above, then the derived mass function imposes that the companion be more massive than 0.017 $M_\odot$. A brown-dwarf companion is expected for orbital inclinations in the range $12.4° \leq i \leq 90°$, $i = 12.4°$ corresponding to the brown-dwarf threshold at $M_2 = 0.079$ $M_\odot$. Such a brown-dwarf companion, if confirmed, would be the most metal-poor ([Fe/H]~ -2.4 as shown in Sect. 3.3) ever discovered, since so far brown-dwarf metallicities are all above [Fe/H]~ -0.6 (Burningham et al. 2014, and references therein), with one possible exception (with a metallicity somewhere between -1 and -2; Burgasser et al. 2003).

2.4.3. Envelope pulsation causing spurious Keplerian-like velocity variations?

Although the Keplerian interpretations presented above are in principle perfectly acceptable, the study of low-metallicity giants by Carney et al. (2003) and by Jorissen et al. (2015) in a companion paper invites us, however, to be cautious.

Among 13 CEMP-(r)s and CH binary systems, Jorissen et al. (2015) have identified two more cases similar to HE 0017+0055, namely HE 1120-2122 and HD 76396, where small-amplitude variations (K ranging from 0.1 to 0.9 km s^{-1}) with periods very close to 1 yr are superimposed on a long-period Keplerian orbit. The CEMP-s star CS 30322-023 shows as well a velocity curve similar to that of HE 0017+0055, with short-term radial-velocity variations with a period of 192 d, and a semi-amplitude of 1.7 km s^{-1}, possibly superimposed on a long-term trend (see Fig. 7 of Masseron et al. 2006).

On the other hand, Carney et al. (2003) reviewed previous evidence that low-metallicity giant stars, especially in globular clusters, systematically exhibit radial-velocity jitter for luminosities near or above the RGB tip (i.e., $M_V \leq -1.5$ or

$\log g \leq 1.3$). A closer look at these velocity variations reveals that they mimick Keplerian variations, with semi-amplitudes of the order of 1 – 1.5 km s^{-1} and periods of the order of 170 - 190 d. Among the cases reported above for CEMP-(r)s/CH systems, only CS 30322-023 conforms to those properties, the other systems being of lower amplitude and longer period. It is likely, however, that those were out of reach with the spectrograph used by Carney et al. (2003).

An important property of the velocity variations reported by Carney et al. (2003) is that they are correlated with low-amplitude photometric variations: *Hipparcos* observations of HD 3008 and HD 110281 in Carney's sample for example revealed them to be variables with (peak-to-peak) amplitudes $A = 0.134 \pm 0.045$ mag and $A = 0.195 \pm 0.032$ mag, respectively. Most importantly, the photometric and radial-velocity data appear to vary with the same period.

Photometric data for HE 0017+0055 are available from the ASAS-3 survey (Pojmanski 1997), and are displayed in Fig. 3, folded on the radial-velocity period of 384 d. No significant modulation has been detected at a 3σ level of 0.03 mag (where $\sigma = 0.01$ mag is the typical error bar on the light curve in Fig. 3). Thus, one may exclude (sinusoidal) variations with a peak-to-peak amplitude larger than $0.03 \times 2\sqrt{2} = 0.08$ mag in HE 0017+0055.

Should the radial-velocity variations be due to stellar oscillations, they would not contradict the absence of ligh-variability detection. Indeed, from a simple linear theory of oscillations, Kjeldsen & Bedding (1995) relate the standard deviation σ_λ (in millimag) of the light variations at wavelength λ (in nm) to the radial-velocity standard deviation $\sigma(\mathrm{V}_r)$ (in km s^{-1}) caused by adiabatic acoustic oscillations. They find the relation:

$$\frac{\sigma_\lambda}{\sigma(\mathrm{V}_r)} = \frac{21.8}{(\lambda/550)(T_{\rm eff}/5777)^2}. \quad (1)$$

Considering the 0.6 km s^{-1} semi-amplitude K of the velocity variations which turns into $\sigma(\mathrm{V}_r) = K/\sqrt{2} = 0.42$ km s^{-1}, the above relation predicts $\sigma_V = 18$ millimag, which is smaller than the detection threshold for the ASAS data estimated above. Thus, the hypothesis that the short-term velocity variations are due to stellar oscillations is consistent with the absence of large light variations in the ASAS light curve.

The expected level of photometric variability in giant stars just below the tip of the red giant branch, where HE 0017+0055 seems to be located (Sect. 5), has been investigated as well by Kiss & Bedding (2003) for the Large Magellanic Cloud. These authors conclude that most of these stars are variable, but with variability (peak-to-peak) amplitudes generally smaller than 0.14 mag. Remember that the ASAS-3 survey puts an upper limit on the (peak-to-peak) variability amplitude of HE 0017+0055 at 0.08 mag.

In the absence of more accurate photometric data for HE 0017+0055, we cannot be sure that the short-term radial-velocity variations are associated to some kind of envelope pulsations. However, the accumulation of systems among CEMP-(r)s/CH stars with low-amplitude velocity variations on a time scale of 190 to 380 d is puzzling and invites us to be cautious, but at this stage we should not exclude any of the three possibilities described in this and the previous sections.

3. Stellar parameters

We now turn to a description of the atmospheric parameters of HE 0017+0055, necessary to perform the abundance analysis which will reveal the CEMP-rs nature of HE 0017+0055. But we present first a description of its kinematical properties, because these properties will guide the derivation of the star's surface gravity.

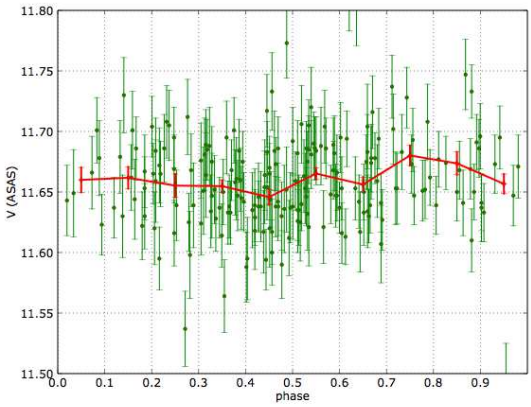

Fig. 3. Photometric data ('grade A' only) from the ASAS-3 catalogue for HE 0017+0055 = ASAS 002022+0112.1, folded on the 383 d period inferred from the radial-velocity variations. The span of the ordinate axis has been set in such a way to eliminate outlying data points. The red curve with error bars corresponds to the average values of the V magnitude in bins of width 0.1 in phase, after eliminating outlying points (i.e., those outside the graphical window). The error bars along that curve correspond to the error on the mean, i.e., the standard dispersion in the considered bin divided by $\sqrt{N}$, where N is the number of data points in the bin.

3.1. Kinematics

The Tycho-2 project (Høg et al. 2000) derived the proper-motion values $\mu_\alpha \cos\delta = 6.9 \pm 2.7$ mas yr^{-1} and $\mu_\delta = -14.2 \pm 2.5$ mas yr^{-1}. These proper motions (along with the radial velocity of −80 km s^{-1}; see Table 1) have been converted into space velocities U, V, W, as this will be the basis for an important argument in the choice of the atmospheric parameters. U, V, W are the heliocentric velocity components along the Galactic coordinate system (U is positive in the direction of the Galactic centre, and V is positive in the direction of Galactic rotation $l = +90°$). Adopting different possible locations for HE 0017+0055 in the Hertzsprung-Russell diagram (on the asymptotic giant branch, on the giant branch, or on the main sequence, along the evolutionary track of a 0.9 $M_\odot$ star of metallicity [Fe/H] = -2.4; Table 3), the corresponding luminosities yield distances that are used to convert the Tycho-2 proper motions into components of the space velocity. In this way, we link the atmospheric gravity $\log g$ with the space velocity.

The results are listed in Table 3 and reveal that for gravities lower than $\log g = 0.5$, the space velocity is uncomfortably large, since it is likely to exceed the Galactic escape velocity[2]. In the solar neighbourhood, the Galactic escape velocity is estimated to be about 500 – 600 km s^{-1} (Smith et al. 2007), but it must be smaller in the halo at the distance of HE 0017+0055 (we will show later that the star is unlikely to be a main-sequence star; hence, it must be located at a large Galactic scale height). The U, V, W velocities obtained for $\log g = 1$ (Table 3) are consistent

[2] See Pereira et al. (2012) for a case study of high-velocity CH stars (HD 5223 and BD -32°1346), near or above the Galactic escape velocity.

Table 3. Kinematical properties of HE 0017+0055, for different hypotheses about its absolute visual magnitude M_V and hence distance, adopting the Tycho-2 proper motion and a V magnitude of 11.65 (Høg et al. 2000, in agreement with the ASAS-3 data; see Fig. 3). The uncertainties on the space motion originate from the uncertainties on the Tycho-2 proper motion. The correspondence between M_V and $\log g$ is from the STAREVOL track (see Sect. 5) for a 0.9 $M_\odot$ star with [Fe/H] = −2.4, [C/H] = −0.7, and C/O = 20, adopting a bolometric correction of 0.3. The first line corresponds however to the Padova track used by Kennedy et al. (2011). U, V, W are the heliocentric velocity components along the Galactic coordinate system (U is positive in the direction of the Galactic centre, and V is positive in the direction of Galactic rotation $l = +90°$). $V_{\alpha*}$ and V_δ are the space velocities along the direction of right ascension and declination, respectively.

$T_{\rm eff}$ (K)	$\log g$	L ($L_\odot$)	M_V	d (kpc)	$\lvert z\rvert$ (kpc)	$V_{\alpha*}$ (km s^{-1})	V_δ (km s^{-1})	U (km s^{-1})	V (km s^{-1})	W (km s^{-1})	lum. class	model
4185	0.18	4470	−4.1	14	12.2	458 ± 179	942 ± 166	68	-956	-433	II	PADOVA
3950	0.5	1920	−3.2	9.3	8.1	305 ± 119	628 ± 111	49	-647	-264	II	STAREVOL
4000	1.0	523	−1.8	4.8	4.2	157 ± 69	296 ± 64	29	-348	-110	III	STAREVOL
3950	4.9	0.03	8.8	0.037	0.032	1.2 ± 0.5	0.15 ± 0.03	12	-40	68	V	STAREVOL

with a typical halo population, since $V \sim -350$ km s^{-1} combined with its estimated metallicity [Fe/H]= −2.4 (see below) locates HE 0017+0055 right along the trend observed by Carney et al. (1996) for halo stars (see their Figs. 1, 3, 5, and 8).

3.2. Atmospheric parameters: previous studies

Kennedy et al. (2011) have derived atmospheric parameters for HE 0017+0055: the effective temperature $T_{\rm eff}$ = 4185 K has been estimated from the ($T_{\rm eff}$, $V - K$) relationship of Alonso et al. (1996), with $V - K$ = 2.96, K being adopted from the 2MASS catalogue (J = 9.31 ± 0.03, H = 8.70 ± 0.03, K = 8.50 ± 0.02; Cutri et al. 2003), and V = 11.459 ± 0.008 and B = 12.991 ± 0.013 from Beers et al. (2007), yielding $B - V$ = 1.532.

Kennedy et al. (2011) estimated the surface gravity to be $\log g$ = 0.18, because that value matches $T_{\rm eff}$ = 4185 K on the Padova evolutionary tracks for the inferred metallicity of [Fe/H]= −2.5 (Girardi et al. 2000; Marigo et al. 2001), *thus assuming that the star lies on the giant branch* and neglecting the possibility that it could be a dwarf carbon star. Uncertainties in $T_{\rm eff}$ and $\log g$ are 100 K and 0.5 dex, respectively. The microturbulence is taken to be 2 km s^{-1}, consistent with previously determined microturbulence values for giant CEMP stars (Johnson et al. 2007; Aoki et al. 2007). We showed in Sect. 3.1 that a low gravity yields an unrealistic value for the space motion of HE 0017+0055 (since the inferred high luminosity puts the star at a distance of 14 kpc; Table 3), and warrants a revised analysis of the atmospheric parameters as presented in Sect. 3.3.

Adopting nevertheless the above atmospheric parameters, Kennedy et al. (2011) estimated a metallicity [Fe/H]= −2.72 for HE 0017+0055, based on a fit of selected Ca and Fe lines with synthetic spectra (see Beers et al. 2007). Kennedy et al. (2011) also derived [C/H]= −0.41, [C/Fe]= 2.31, [N/Fe]= 0.52, [O/H]= −1.7, and [O/Fe]= 1.0 (corresponding to $\log \epsilon$(C) = 8.02, $\log \epsilon$(N) = 5.64, $\log \epsilon$(O) = 6.99, adopting $\log \epsilon_\odot$(C) = 8.43, $\log \epsilon_\odot$(N) = 7.83, and $\log \epsilon_\odot$(O) = 8.69 for the Sun; Asplund et al. 2009). In this paper, we use the standard notation $\log \epsilon(X) = \log[n(X)/n(H)] + 12$, where $n(X)$ is the number density of element X. The CNO abundances of HE 0017+0055 appear normal among CEMP stars (see, e.g., Fig. 18 of Masseron et al. 2010). Adopting the solar CNO abundances as listed above [corresponding to $(C/O)_\odot$ = 0.55], one thus finds C/O= 10.7 for HE 0017+0055. Goswami (2005) moreover finds a very low $^{12}C/^{13}C$ ratio of 1.3, typical of (or even lower than) the CN-cycle equilibrium value. This value is the lowest among those reported by both Goswami (2005) and Masseron et al. (2010).

Nothing is known about the s-process content of HE 0017+0055; this issue will therefore be investigated as well in Sect. 4.

3.3. Atmospheric parameters revisited

We re-derived the atmospheric parameters of HE 0017+0055 for the reasons given in Sect. 3.2. We first tried to use the relation between $(V-K)$, $(H-K)$, $(J-K)$ and $T_{\rm eff}$ derived by Bergeat et al. (2001) for carbon stars to estimate the effective temperature. Unfortunately, the photometric indices for HE 0017+0055 ($V-K$ = 2.96 ± 0.03, $H - K$ = 0.20 ± 0.05, $J - K$ = 0.81 ± 0.05) require to severely extrapolate the calibrations of Bergeat et al. (2001), which were aimed at cool carbon stars of type N. Taken at face value, these calibrations yield temperatures of 4680, 3470, and 3890 K, respectively, and are thus of little use. We note, however, that HE 0017+0055 has colours identical to those of the warm R stars studied by Zamora et al. (2009) (see their Fig. 1). In that sample, HIP 87603 and HIP 113150 share the same $H - K$ and $J-K$ indices as HE 0017+0055, and have effective temperatures of 4100 and 4500 K respectively (and both with $\log g$ = 2.0).

The photometric similarity between HE 0017+0055 and both R and CH stars[3] (Zamora et al. 2009) led us to focus our search around $T_{\rm eff} \sim 4100 - 4500$ K and $\log g$ = 2.0. The final atmospheric parameters were derived by an iterative process of fitting specific spectral regions and fine-tuning the parameters consecutively, modifying $T_{\rm eff}$, gravity, metallicity, s-process abundances as a whole, and the CNO abundances until a reasonable fit to the observed spectrum was found, for the whole range 420 – 800 nm. The synthetic spectra were produced by the TURBOSPECTRUM code (Alvarez & Plez 1998) from carbon-enhanced model atmospheres with the C, N and O abundances iteratively adapted to the values found in HE 0017+0055. The model atmospheres were computed with the opacity sampling technique usual for the MARCS models (Gustafsson et al. 2008), and using opacity tables with variable C, N and O abundances.

The wings of the Balmer lines were fitted, as well as those of strong lines like Ca I λ 422.67 nm (Fig. 4). Although the gravity

[3] We note, however, that given the strong CH band at 437.0 nm present in HE 0017+0055, it is clear that the star must be considered as a CH star (see Fig. 1e of Barnbaum et al. 1996). The atmospheric parameters of CH and R stars are anyway very similar.

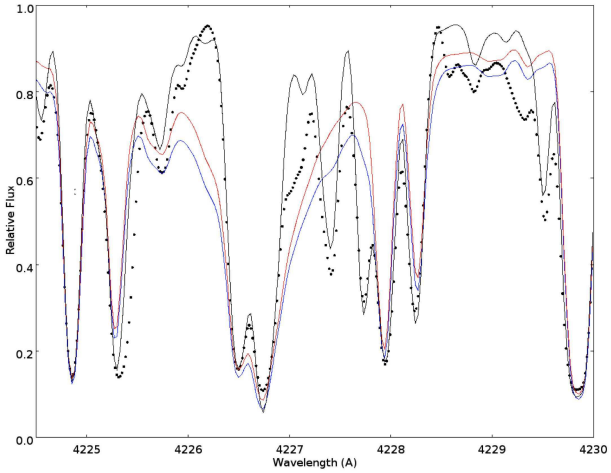

Fig. 4. Effect of gravity on the Ca I λ 422.67 nm line (black curve: $\log g$ = 1 and [Fe/H] = −2.4 dex; blue curve: $\log g$ = 5 and [Fe/H] = −2.4 dex; red curve: $\log g$ = 5 and [Fe/H] = −3.5 dex). Except otherwise stated, the atmospheric parameters used to generate the synthetic spectra are those listed in Table 4.

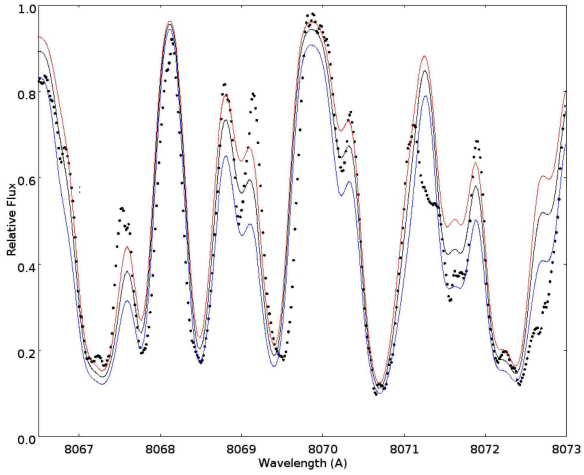

Fig. 7. Intensities of lines from the CN band around λ8070 Å, showing the impact of the N abundance [with $\log \epsilon$(C) fixed at 8.2]: $\log \epsilon$(N) = 7.7 (red curve), $\log \epsilon$(N) = 7.9 (black curve), $\log \epsilon$(N) = 8.2 (blue curve). Except otherwise stated, the atmospheric parameters used to generate the synthetic spectra are those listed in Table 4.

and s-process overall abundances are entangled (s-process elements often involve lines from the singly ionized species, which are generally strengthened in low-density atmospheres), a solution with [s/Fe] = +2.0 dex[4] (or even more, except for the first s-process-peak element Y) and $\log g$ = 1 represents a good overall match to the spectrum, as shown in Fig. 5 in a region containing many lines from singly-ionized s-process elements. We stress that the shape of the $^{12}C^{13}C$ and $^{13}C^{13}C$ bandheads around 474.0 nm are quite sensitive to gravity (see Fig. 6), and it is this criterion that led us to adopt $\log g$ = 1.

HE 0017+0055 cannot be a low-metallicity carbon dwarf, since even at such a low metallicity, the wings of the more intense lines would be too strong. Fig. 4 reveals the impact of gravity on the Ca I λ 422.67 nm line. At higher gravities, the wings of the line become stronger, and metallicity has to be decreased (to [Fe/H]= −3.5), but then other (metallic) lines start becoming really weak, and make this solution unacceptable.

Especially noteworthy is the fact that HE 0017+0055 combines features from both J stars (a low $^{12}C/^{13}C$ ratio, as inferred from the $^{12}C^{13}C$ and $^{13}C^{13}C$ bandheads around 474.0 nm; see Fig. 6) and CH stars (large s-process overabundances, and strong CH bands in the region 430 - 440 nm, caused by a large C overabundance and a very low metallicity [Fe/H] = -2.4). The high N abundance, as derived from the CN band longward of 570 nm or 800 nm (Fig. 7), is also remarkable, and is consistent with the low $^{12}C/^{13}C$ ratio ($\sim$ 4), since both features are signatures of CN-processing, as it may occur along the red giant branch, with extra-mixing bringing these products to the stellar surface (Placco et al. 2014). The N overabundance ([N/H] = 0.07, [C+N/H] = 0.85, and [C/N] = 0.16) is in fact typical of CEMP-rs stars (we will show in Sect. 4 that HE 0017+0055 is indeed a CEMP-rs star), as may be seen from Fig. 17 of Masseron et al. (2010). With the adopted atmospheric parameters, there seems to be no way of avoiding a strong N overabundance if the strengths of the CN lines are to be reproduced. The carbon abundance of HE 0017+0055 ([C/H] = -0.23) seems reasonable as well among CEMP-rs stars (Fig. 14 from Masseron et al. 2010).

In conclusion, HE 0017+0055 must thus be considered as another member of the CEMP class, albeit one of the coolest and most luminous member of the class, but not as extreme as CS 30322-023, the latter having atmospheric parameters $T_{\rm eff}$ = 4100 K, $\log g \leq -0.3$, and [Fe/H]= −3 (Masseron et al. 2006). The atmospheric parameters of HE 0017+0055 are used in Sect. 4 to derive abundances for s-process elements. The evolutionary status of HE 0017+0055 is discussed next (Sect. 5).

4. Heavy-element abundances

A detailed analysis of abundances for some key elements (some typical of the s-process, others typical of the r-process) has been performed using the parameters from Table 4, using the Keck/Hires spectrum obtained on October 7, 2008 and reduced using the standard "Makee" pipeline. The line list is given in Table A.1, avoiding spectral regions with the unaccounted SiC_2 Merrill-Sanford bands. Oscillator strengths are from the VALD database (Kupka et al. 2011). The corresponding abundances are listed in Table 5. The carbon-star model used has [Fe/H]= −2, $T_{\rm eff}$ = 4250 K, $\log g$ = 1.00, [α/Fe] = +0.4, ξ_t = 2.0 km s^{-1}, $\log \epsilon$(C) = 8.2, $\log \epsilon$(N) = 7.4, $\log \epsilon$(O) = 7.1, [s/Fe] = +2.0 dex. The synthetic spectrum was convolved with a macroturbulence velocity of 8.0 km s^{-1}. An analysis of the sensitivity of the Fe, Zr and Eu abundances to the atmospheric parameters is presented in Table 6. The global uncertainty, adding up all individual uncertainties, is on the order of ±0.3 dex for the heavy elements Zr and Eu. This is somewhat larger than usual, but is nevertheless of the same order as the uncertainties found by Zamora et al. (2009) in their analysis of R-type carbon stars, thus revealing the difficulties inherent in the analysis of carbon stars.

The correct Ce abundance was used when deriving the Li abundance, since the Ce II line at λ 6708.099 blends the Li I resonance doublet at λ 6707.706 and 6707.91 (Reyniers et al. 2002). Only an upper limit could be set on the Li abundance: $\log \epsilon$(Li) < 1.0. This star is thus not Li-rich.

[4] This means that all heavy elements with the s-process contributing more than 50% of their solar-system abundance were assigned an overabundance of 2.0 dex in the spectral-synthesis computation.

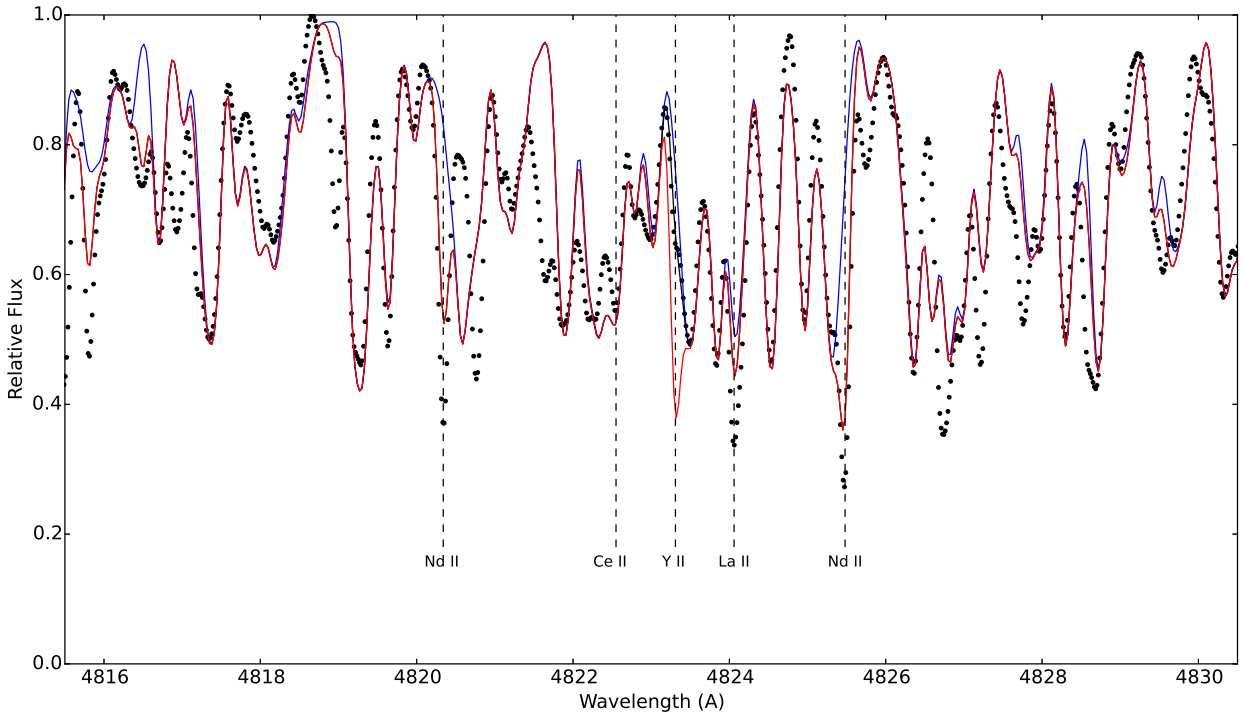

Fig. 5. The effect of a general increase by 2.0 dex of s-process elements (red line), as compared to their solar abundances (blue line). Compare with Fig. 5 of Reyniers et al. (2007). Note that the Y II line around 4823.3 Å is not as enhanced as the other s-process lines (red line). A better match to the Y abundance is obtained with [Y/Fe] = 0.5 dex (black line). Except otherwise stated, the atmospheric parameters used to generate the synthetic spectra are those listed in Table 4.

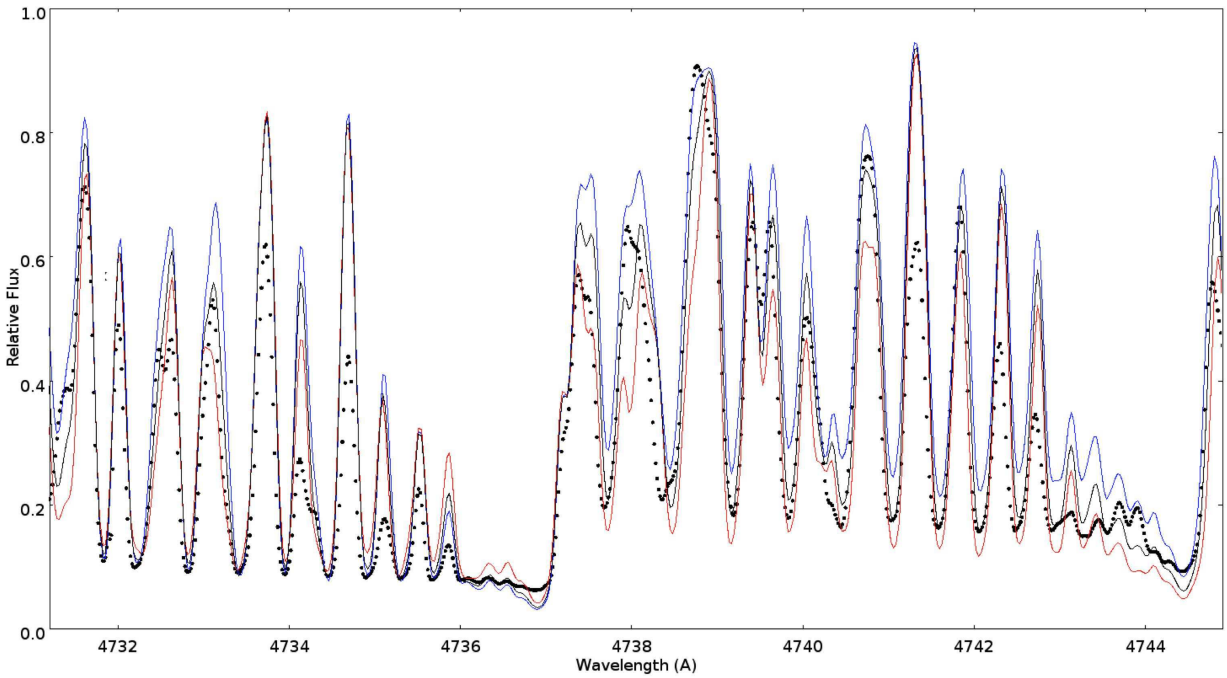

Fig. 6. The $^{12}C^{13}C$ and $^{13}C^{13}C$ band heads around 474.0 nm (with $\log \epsilon(C) = 8.2$ and $\log \epsilon(N) = 7.9$), for $^{12}C/^{13}C = 2$ (red curve), 4 (black curve), and 7 (blue curve). Except otherwise stated, the atmospheric parameters used to generate the synthetic spectra are those listed in Table 4.

Table 4. Adopted atmospheric parameters of HE 0017+0055 (ξ_t is the microturbulence).

$T_{\rm eff}$	$\log g$	[Fe/H]	$\log\epsilon$			[X/H]			$^{12}C/^{13}C$	[s/Fe]	ξ_t
(K)			C	N	O	C	N	O			(km s^{-1})
4250 ± 100	1 ± 1	-2.4	8.2 ± 0.1	7.9 ± 0.1	7.1[a]	−0.23	2.1	−1.6[a]	4 ± 1	2.0 ± 0.2	2

[a] oxygen abundance imposed from [O/Fe] = 0.8 (see Fig. 18 of Masseron et al. 2010).

Table 5. Abundances (in the scale $\log\epsilon$(H) = 12) of Fe and heavy elements, the line-to-line standard deviation is between parenthesis. *N* is the number of lines used in the computation of the average abundance. Abundances have been normalized by the solar photospheric values from Asplund et al. (2009).

X	$\log\epsilon$(X)	[X/H]	[X/Fe]	*N*
Fe	5.02 (0.07)	-2.4	-	6
Y II	0.33 (0.03)	-1.9	0.5	2
Zr II	1.73 (0.04)	-0.9	1.6	4
La II	1.12 (0.13)	0.0	2.4	5
Ce II	1.22 (0.06)	-0.5	2.0	3
Nd II	1.20 (0.06)	-0.3	2.2	7
Sm II	0.43 (0.03)	-0.6	1.9	2
Eu II	0.35 (0.05)	-0.2	2.3	2
Dy II	-0.10 (0.20)	-1.2	1.2	2
Er II	0.25 (0.05)	-0.7	1.8	2

As can be seen from Table 5, the heavy-element abundance pattern in HE 0017+0055 looks at first sight typical of a CEMP-s star, with moderate overabundances for elements belonging to the first s-process peak (Y, Zr), and stronger overabundances for the second peak (La, Ce, Nd). However, the analysis of the r-process elements Sm, Eu, Dy and Er reveals that they are enriched as well, and therefore HE 0017+0055 is likely a CEMP-rs star. The defining criterion of a CEMP-rs star is based on the [Ba/Eu] ratio being in the range 0.0 – +0.5 dex, whereas [Ba/Eu] > 0.5 dex for CEMP-s stars (Beers & Christlieb 2005, see also Figs. 1 and 2 of Masseron et al. 2010). Unfortunately, the Ba abundance could not be derived safely, because the 493.407, 585.37 and 614.14 nm lines were either blended or with strong and badly fitted wings. Nevertheless, a lower limit on the Ba abundance could be set at $\log\epsilon$(Ba) > 1.6 dex (using the 493.407 and 614.14 nm lines), corresponding to [Ba/H] > −0.6 and [Ba/Fe] > 1.9. Combined with [Eu/Fe] = 2.3 dex (Table 5), these values confirm the CEMP-rs nature of HE 0017+0055 (see also Fig. 1 of Masseron et al. 2010). In that respect, it is noteworthy that the [La/Ce] ratio (0.5 dex) is much larger than the typical (negative) values predicted by the computations of Goriely & Siess (2005) from the operation of the $^{13}C(\alpha, n)^{16}O$ neutron source in low-mass AGB stars. The larger [La/Ce] values observed in HE 0017+0055 as in all the other CEMP-rs stars are thus a strong indication that the $^{13}C(\alpha, n)^{16}O$ neutron source does not operate in those stars, as suggested by Masseron et al. (2010). It is also meaningful that the [La/Ce] values observed in CEMP-rs stars are compatible with the values 0.2–0.4 dex predicted from the operation of the $^{22}Ne(\alpha, n)^{25}Mg$ neutron source in warm pulses, and after dilution in the AGB envelope (Goriely & Siess 2005).

Unfortunately, the abundance of Pb, falling in the third s-process peak and generally much enhanced in CEMP-rs stars, could not be easily derived, as the Pb blend is not cleanly reproduced.

Only an upper limit could be set on the technetium abundance ($\log\epsilon$(Tc)< 0.0), which hints at the absence of Tc, thus confirming the extrinsic nature of HE 0017+0055.

5. The evolutionary status of HE 0017+0055

Being of very low metallicity, the star must have formed in the early stage of the Galaxy: according to Fig. 2 of Freeman & Bland-Hawthorn (2002), stars with metallicities [Fe/H]= −2.4 like HE 0017+0055 formed about 13 Gyr ago. Since HE 0017+0055 is located on the giant branch, it must have spent about 12 Gyr on the main sequence (and the remainder in post-main-sequence phases) and must therefore have had an initial mass of about 0.9 $M_\odot$. The gravity and effective temperatures of HE 0017+0055 mentioned in Sect. 3 may be combined, along with the above mass estimate (0.9 $M_\odot$), to derive the luminosity:

$$\log L/L_\odot = \log M/M_\odot + 4\log T_{\rm eff}/T_{\rm eff,\odot} - \log g/g_\odot = 2.86, \quad (2)$$

corresponding to L = 724 $L_\odot$, in agreement with the prediction of the STAREVOL C-rich model described below (and Table 3). According to the compilation of CEMP-star properties by Masseron et al. (2010), this value for the luminosity makes HE 0017+0055 one the brightest CEMP stars (their Fig. 12), just below CS 30322-023 (Fig. 8 and Masseron et al. 2006). The radius corresponding to HE 0017+0055 gravity and adopted mass is 50 $R_\odot$. Only CS 30322-023, with $\log g = -0.3 \pm 0.3$ and $T_{\rm eff}$ = 4100 - 4350 K (Masseron et al. 2006), has a higher luminosity among CEMP stars. Although CS 30322-023 most likely lies above the RGB tip (Fig. 8), and might therefore belong to the rare class of low-metallicity AGB stars, this is not required for HE 0017+0055.

Fig. 8 presents evolutionary tracks of a 0.9 $M_\odot$ star with a metallicity [Fe/H]= −2.4 like HE 0017+0055 computed with the STAREVOL code (Siess & Arnould 2008). The exact location of the giant branch in the Hertzsprung-Russell diagram is sensitive to the opacity in the atmosphere, and hence to the carbon- or oxygen-rich nature of the star (Marigo 2002). For a star strongly enriched in carbon as is HE 0017+0055, the evolutionary track is shifted towards lower temperatures, thus counteracting to some extent the blueward shift due to the low metallicity. This effect appears crucial to derive atmospheric parameters consistent with the ones derived from the spectral analysis in Sect. 3.3, and especially to avoid the high luminosities that would yield large space motions.

The distance of HE 0017+0055 may then be estimated, adopting the same bolometric correction of 0.3 as that estimated by Masseron et al. (2006) for CS 30322-023, a distance of 4.8 kpc is obtained (Table 3). At such a distance, the Tycho-2 proper motions (see Sect. 3.1) translate into large space velocities as listed in Table 3[5]. As discussed in Sect. 3.1, these space velocities are consistent with HE 0017+0055 being a normal member of the Galactic halo.

An accurate trigonometric parallax for HE 0017+0055 should become available from Gaia within a few years time and should provide a conclusive answer to the discussion on the distance and evolutionary stage of this star.

[5] A similar analysis is unfortunately not possible for CS 30322-023 for which no proper motion is available.

Table 6. Sensitivity of the derived abundances (in dex) on the atmospheric parameters. For non-symmetrical abundance variations, the largest value is listed. The final uncertainty on the abundance is computed by quadratically adding all the uncertainties, including the standard deviation from the line-to-line scatter.

Element	$T_{\rm eff}$ ±100 K	log g ±0.5	[Fe/H] ±0.25 dex	ξ ±1 km s^{-1}	macro. ±1 km s^{-1}	Total (dex)
Fe	±0.09	±0.07	–	±0.12	±0.03	±0.18
Zr	±0.20	±0.11	±0.07	±0.08	±0.11	±0.29
Eu	±0.20	±0.15	±0.20	±0.10	±0.07	±0.34

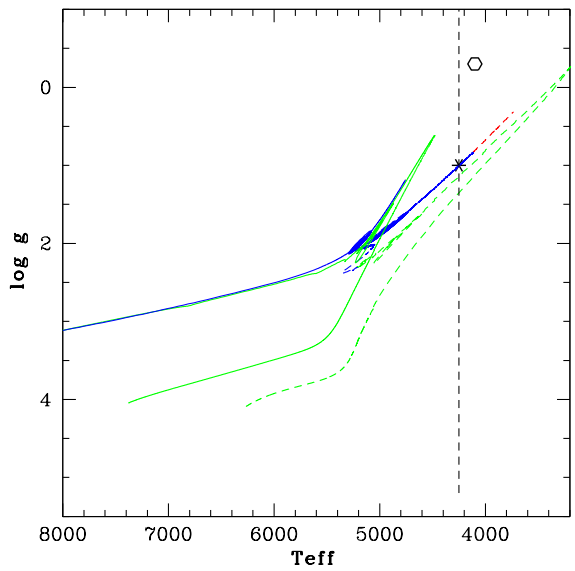

Fig. 8. Evolutionary track in the ($T_{\rm eff}$, log g) diagram for a 0.9 $M_{\odot}$ star of metallicity [Fe/H] = -2.4, computed with the STAREVOL code, with an atmosphere being either oxygen-rich (solid track) or carbon-rich (dashed track, corresponding to $\log \epsilon(C) = 8.2$ or [C/H] = −0.23). The oxygen-rich track is limited to the giant and horizontal branches (green and blue parts of the track, respectively), for the sake of clarity, whereas the carbon-rich track includes as well the asymptotic giant branch (red part of the track). The vertical dashed line corresponds to $T_{\rm eff}$ = 4250 K. The location of HE 0017+0055 as inferred from the parameters of Table 4 is indicated by the star symbol, whereas that of CS 30322-023 is indicated by the open circle.

6. Conclusions

The radial-velocity monitoring of HE 0017+0055 revealed short-term variations superimposed on a long-term trend. The short-term variations are characterised by a period of 383 d and a very small mass function of $(6.1\pm1.1)\times10^{-6}$ $M_{\odot}$. There are three possible explanations for these low-amplitude variations: (i) orbital variations caused by a WD companion in a very inclined orbit ($i \sim 2.3°$), (ii) orbital variations caused by a brown dwarf in a moderately inclined orbit ($12.4° \leq i \leq 90°$), (iii) velocity jitter reported by Carney et al. (2003) as typical in low-metallicity giants close to the RGB tip. Jorissen et al. (2015) report three more cases among CH/CEMP-s systems of small-amplitude velocity variations with periods close to 1 yr, very similar thus to the one observed in HE 0017+0055. A definite conclusion as to which possibility is the valid one must await the results of an accurate photometric monitoring, since the variations are expected to be minute (a few hundredths of a magnitude).

An abundance study has shown that HE 0017+0055 is not only enriched in s-process elements but also in r-process elements (at levels on the order of 2 dex for most of them), and may thus be flagged as a CEMP-rs star. A mass-transfer scenario is generally invoked to account for the abundance peculiarities of CEMP-rs stars. In this scenario, the CEMP-rs star has been polluted by heavy-element-rich matter coming from a companion formerly on the thermally-pulsing AGB star (most probably a massive one; Masseron et al. 2010), now a WD. In case (i) above, the WD is in the inner orbit, and the outer orbit hosts an innocent bystander star, whereas in cases (ii) and (iii), the WD is in the long-period orbit. Although the outer orbit must have a period of several decades, this is still compatible with the mass-transfer scenario, since other s-process-polluted systems with similarly long orbital periods are known (like HD 26; Jorissen et al., 2015).

Acknowledgements. This research has been funded by the Belgian Science Policy Office under contract BR/143/A2/STARLAB. SvE and LS are FNRS research associates. The work of T.T.H. was supported by Sonderforschungsbereich SFB 881 "The Milky Way System" (subproject A4) of the German Research Foundation (DFG). J.A. and B.N. gratefully acknowledge financial support from the Danish Natural Science Research Council and the Carlsberg Foundation. Based on observations obtained with the HERMES spectrograph, supported by the Fund for Scientific Research of Flanders (FWO), the Research Council of K.U.Leuven, the Fonds National de la Recherche Scientifique (F.R.S.-FNRS), Belgium, the Royal Observatory of Belgium, the Observatoire de Genève, Switzerland and the Thüringer Landessternwarte Tautenburg, Germany.

References

Abate, C., Pols, O. R., Izzard, R. G., Mohamed, S. S., & de Mink, S. E. 2013, A&A, 552, A26
Alonso, A., Arribas, S., & Martinez-Roger, C. 1996, A&A, 313, 873
Alvarez, R., & Plez, B. 1998, A&A, 330, 1109
Alvarez, R., Mennessier, M.-O., Barthes, D., Luri, X., & Mattei, J. A. 1997, A&A, 327, 656
Aoki, W., Beers, T. C., Christlieb, N., et al. 2007, ApJ, 655, 492
Asplund, M., Grevesse, N., Sauval, A. J., & Scott, P. 2009, ARA&A, 47, 481
Barbuy, B., Cayrel, R., Spite, M., et al. 1997, A&A, 317, L63
Barbuy, B., Spite, M., Spite, F., et al. 2005, A&A, 429, 1031
Barnbaum, C., Stone, R. P. S., & Keenan, P. C. 1996, ApJS, 105, 419
Beers, T. C., & Christlieb, N. 2005, ARA&A, 43, 531
Beers, T. C., Flynn, C., Rossi, S., et al. 2007, ApJS, 168, 128
Beers, T. C., Sivarani, T., Marsteller, B., et al. 2007, AJ, 133, 1193
Bergeat, J., Knapik, A., & Rutily, B. 2001, A&A, 369, 178
Buchhave, L. A., Bakos, G. Á., Hartman, J. D., et al. 2010, ApJ, 720, 1118
Burgasser, A. J., Kirkpatrick, J. D., Burrows, A., et al. 2003, ApJ, 592, 1186
Burningham, B., Smith, L., Cardoso, C. V., et al. 2014, MNRAS, 440, 359
Carney, B. W., Latham, D. W., Stefanik, R. P., Laird, J. B., & Morse, J. A. 2003, AJ, 125, 293
Carney, B. W., Laird, J. B., Latham, D. W., & Aguilar, L. A. 1996, AJ, 112, 668
Carollo, D., Freeman, K., Beers, T. C., et al. 2014, ApJ, 788, 180
Christlieb, N., Green, P. J., Wisotzki, L., & Reimers, D. 2001, A&A, 375, 366
Constantino, T., Campbell, S., Gil-Pons, P., & Lattanzio, J. 2014, ApJ, 784, 56
Cutri, R. M., Skrutskie, M. F., van Dyk, S., et al. 2003, 2MASS VizieR Online Data Catalog, II/246
Eggleton, P. P. 1983, ApJ, 268, 368
Fabrycky, D., & Tremaine, S. 2007, ApJ, 669, 1298
Freeman, K., & Bland-Hawthorn, J., 2002, ARA& A 40, 487
Girardi, L., Bressan, A., Bertelli, G., & Chiosi, C. 2000, A&AS, 141, 371
Goriely, S., & Siess, L. 2005, in From Lithium to Uranium: Elemental Tracers of Early Cosmic Evolution, eds. V. Hill, P. François, & F. Primas, IAU Symp. 228, pp.451-460

Gorlova, N., Van Winckel, H., Vos, J., et al. 2013, EAS Publication Series, 64, 163
Goswami, A. 2005, MNRAS, 359, 531
Gustafsson, B., Edvardsson, B., Eriksson, K., et al. 2008, A&A, 486, 951
Hansen, T., Andersen, J., Nordström, B., Buchhave, L. A., & Beers, T. C. 2011, ApJ, 743, L1
Hansen, T., Hansen, C. J., Christlieb, N., et al. 2015a, in: Proceedings of the International Symposium Nuclei in the Cosmos 2014, arXiv:1503.01990
Hansen, T., Andersen, J., Nordström, B., Beers, T.C., Placco, V.M., Yoon, J., & Buchhave, L. A. 2015b, A&A, submitted
Hill, V., Barbuy, B., Spite, M., et al. 2000, A&A, 353, 557
Hinkle, K. H., Lebzelter, T., Joyce, R. R., & Fekel, F. C. 2002, AJ, 123, 1002
Høg, E., Fabricius, C., Makarov, V. V., et al. 2000, A&A, 355, L27
Hummel, C. A., Benson, J. A., Hutter, D. J., et al. 2003, AJ, 125, 2630
Johnson, J. A., Herwig, F., Beers, T. C., & Christlieb, N. 2007, ApJ, 658, 1203
Jorissen, A., Van Eck, S., Van Winckel, H., Merle, T., Boffin, H.M.J., Andersen, J. Nordström, J., Udry, S., Masseron, T., Lenaerts, L., Waelkens, C., 2015, A&A, in press
Kennedy, C. R., Sivarani, T., Beers, T. C., et al. 2011, AJ, 141, 102
Kiss, L. L., & Bedding, T. R. 2003, MNRAS, 343, L79
Kjeldsen, H., & Bedding, T. R. 1995, A&A, 293, 87
Kupka, F., Dubernet, M.-L., & VAMDC Collaboration 2011, Baltic Astronomy, 20, 503
Lucatello, S., Tsangarides, S., Beers, T. C., et al. 2005, ApJ, 625, 825
Marigo, P., Girardi, L., Chiosi, C., & Wood, P. R. 2001, A&A, 371, 152
Marigo, P. 2002, A&A, 387, 507
Masseron, T., van Eck, S., Famaey, B., et al. 2006, A&A, 455, 1059
Masseron, T., Johnson, J. A., Plez, B., et al. 2010, A&A, 509, A93
McClure, R. D., & Woodsworth, A. W. 1990, ApJ, 352, 709
Muterspaugh, M. W., Lane, B. F., Fekel, F. C., et al. 2008, AJ, 135, 766
O'Brien, D. P., McAlister, H. A., Raghavan, D., et al. 2011, ApJ, 728, 111
Paczyński, B. 1971, ARA&A, 9, 183
Pereira, C. B., Jilinski, E., Drake, N. A., et al. 2012, A&A, 543, A58
Placco, V. M., Frebel, A., Beers, T. C., & Stancliffe, R. J. 2014, ApJ, 797, 21
Pojmanski, G. 1997, Acta Astron., 47, 467
Raskin, G., van Winckel, H., Hensberge, H., et al. 2011, A&A, 526, A69
Reyniers, M., Van Winckel, H., Biémont, E., & Quinet, P. 2002, A&A, 395, L35
Reyniers, M., Abia, C., van Winckel, H., et al. 2007, A&A, 461, 641
Siess, L. 2001, In: From Darkness to Light: Origin and Evolution of Young Stellar Clusters, T. Montmerle & Ph. André (eds.), ASP Conf. Ser. Vol. 243, 581
Siess, L., & Arnould, M. 2008, A&A, 489, 395
Sivarani, T., Bonifacio, P., Molaro, P., et al. 2004, A&A, 413, 1073
Smith, M. C., Ruchti, G. R., Helmi, A., et al. 2007, MNRAS, 379, 755
Stephenson, C. B. 1985, AJ, 90, 784
Stephenson, C. B. 1989, Publications of the Warner & Swasey Observatory, 3, 53
Sterzik, M. F., & Tokovinin, A. A. 2002, A&A, 384, 1030
Udry, S., Mayor, M., & Queloz, D. 1999, IAU Colloq. 170: Precise Stellar Radial Velocities, 185, 367
Van Winckel, H., Jorissen, A., Gorlova, N., et al. 2010, Mem. Soc. Astron. Italiana, 81, 1022
Wood, P. R. 2000, PASA, 17, 18
Začs, L., Sperauskas, J., Grankina, A., et al. 2015, ApJ, 803, 17
Zamora, O., Abia, C., Plez, B., Domínguez, I., & Cristallo, S. 2009, A&A, 508, 909

Appendix A: Line list for the abundance analysis

Table A.1. Lines used in the metallicity and s-process abundance analysis, and the corresponding abundances (in the scale $\log\epsilon(\mathrm{H}) = 12$). The bold values at the end of each element's list correspond to the average abundance and its corresponding standard dispersion. A vertical bar to the left of the wavelength values groups hyperfine structure and isotopic shifts for a given line.

	λ (Å)	χ_{exc} (eV)	$\log gf$	$\log\epsilon$
Fe I	4466.551	2.831	-0.600	4.9
	4903.310	2.882	-0.926	5.0
	5195.472	4.220	-0.086	5.1
	6219.281	2.198	-2.434	5.0
	6839.830	2.559	-3.350	5.0
	7760.897	5.486	-3.838	5.1
				5.02 (0.07)
Y II	5200.406	0.992	-0.570	0.35
	5205.724	1.033	-0.193	0.3
				0.325 (0.025)
Zr II	4457.413	1.184	-1.220	1.7
	4816.500	1.011	-2.000	1.8
	4831.327	1.208	-1.720	1.7
	4962.310	0.972	-2.000	1.7
				1.73 (0.04)
La II	4558.457	0.321	-0.970	0.9
	4808.996	0.235	-1.40	1.3
	4824.052	0.651	-0.87	1.1
	4920.965	0.126	-2.261	
	4920.965	0.126	-2.407	
	4920.966	0.126	-2.065	
	4920.966	0.126	-2.078	
	4920.966	0.126	-2.738	
	4920.968	0.126	-1.831	
	4920.968	0.126	-1.956	
	4920.968	0.126	-2.629	
	4920.971	0.126	-1.646	
	4920.971	0.126	-1.895	
	4920.971	0.126	-2.650	
	4920.975	0.126	-1.490	
	4920.975	0.126	-1.891	
	4920.975	0.126	-2.760	
	4920.979	0.126	-1.354	
	4920.979	0.126	-1.957	
	4920.979	0.126	-2.972	
	4920.985	0.126	-1.233	
	4920.985	0.126	-2.162	
	4920.985	0.126	-3.375	1.2

Table A.1. Continued

	λ (Å)	χ_{exc} (eV)	log gf	log ϵ
La II	4921.774	0.244	-1.139	
	4921.774	0.244	-2.220	
	4921.774	0.244	-3.601	
	4921.775	0.244	-1.233	
	4921.775	0.244	-2.005	
	4921.775	0.244	-3.207	
	4921.776	0.244	-1.334	
	4921.776	0.244	-1.445	
	4921.776	0.244	-1.915	
	4921.776	0.244	-1.927	
	4921.776	0.244	-2.923	
	4921.776	0.244	-3.010	
	4921.777	0.244	-1.566	
	4921.777	0.244	-1.955	
	4921.777	0.244	-2.939	
	4921.778	0.244	-1.700	
	4921.778	0.244	-1.848	
	4921.778	0.244	-2.006	
	4921.778	0.244	-2.053	
	4921.778	0.244	-2.258	
	4921.778	0.244	-3.123	1.1
				1.12 (0.13)
Ce II	4835.674	0.957	-0.870	1.2
	5187.458	1.212	0.150	1.15
	5191.633	0.869	-0.560	1.3
				1.22 (0.06)
Nd II	4594.447	0.205	-1.360	1.2
	4820.339	0.205	-0.920	1.28
	4825.478	0.182	-0.420	1.2
	4859.026	0.321	-0.440	1.1
	5228.420	0.380	-1.280	1.3
	5249.576	0.976	0.200	1.2
	5276.869	0.859	-0.440	1.15
				1.20 (0.06)
Sm II	4777.840	0.040	-1.420	0.45
	4815.800	0.185	-0.820	0.4
				0.43 (0.03)

Table A.1. Continued

	λ (Å)	χ_{exc} (eV)	log gf	log ϵ
Eu II	4522.486	0.207	-2.159	
	4522.498	0.207	-1.266	
	4522.538	0.207	-1.984	
	4522.549	0.207	-1.474	
	4522.561	0.207	-2.159	
	4522.581	0.207	-1.962	
	4522.590	0.207	-1.711	
	4522.600	0.207	-1.984	
	4522.615	0.207	-2.038	
	4522.621	0.207	-1.980	
	4522.630	0.207	-1.962	
	4522.640	0.207	-2.247	
	4522.644	0.207	-2.256	
	4522.650	0.207	-2.038	
	4522.657	0.207	-2.344	
	4522.661	0.207	-2.247	0.3
	6437.637	1.320	-1.428	
	6437.639	1.320	-2.206	
	6437.635	1.320	-2.206	
	6437.637	1.320	-1.377	
	6437.637	1.320	-2.010	
	6437.635	1.320	-2.010	
	6437.635	1.320	-1.287	
	6437.633	1.320	-1.956	
	6437.633	1.320	-1.956	
	6437.630	1.320	-1.181	
	6437.623	1.320	-1.998	
	6437.627	1.320	-1.998	
	6437.620	1.320	-1.070	
	6437.606	1.320	-2.191	
	6437.617	1.320	-2.191	
	6437.603	1.320	-0.960	0.4
				0.35 (0.05)
Dy II	3984.688	1.752	-0.328	+0.1
	3996.689	0.590	-0.260	-0.3
				-0.10 (0.20)
Er II	3980.144	0.886	-1.004	0.2
	4008.177	0.055	-1.547	0.3
				0.25 (0.05)